Available online at www.sciencedirect.com
SCIENCE DIRECT®
Journal of Chromatography A, 1036 (2004) 205–216
JOURNAL OF CHROMATOGRAPHY A
www.elsevier.com/locate/chroma

# Resolution of overlapped non-absorbing and absorbing solutes using either an absorption null-balance detection window or multivariate deconvolution applied to capillary electrophoresis of anionic surfactants

Virginia Bernabé-Zafón [a], José R. Torres-Lapasió [a], Silvia Ortega-Gadea [b], Ernesto F. Simó-Alfonso [a], Guillermo Ramis-Ramos [a,*]

[a] *Departament de Química Analítica, Facultad de Química, Universitat de València, Dr. Moliner 50, Burjassot, Valencia 46100, Spain*
[b] *Químicas Oro S.A., CV-35, Sant Antoni de Benaixever 46184, Spain*

Received 8 December 2003; received in revised form 8 March 2004; accepted 9 March 2004

**Abstract**

Non-absorbing alkyl ether sulfates (AES) can be separated using anthraquinone-2-carboxylic acid (AQCA) as a probe; however, absorbing alkyl benzene sulfonates (ABS), if present, interfere indirect detection of most AES oligomers. Overcoming of this interference, as well as the simultaneous characterisation and evaluation of AES, fatty acids and ABS, was accomplished by using a diode-array detector and the procedures here discussed. First, it was shown that ABS can be made undetectable by using a 9 nm wide and 227 nm centred charge-absorptivity null-balance detection window (NBDW), where its contribution to the absorbance cancels the dilution effects that its presence induces on the signal of the background chromophore (BGC). Two other procedures, not requiring any prior knowledge on the nature of the absorbing interference, were also addressed. In the first one, the NBDW procedure was emulated by software, by treating the time–wavelength data matrix stored during the experimental run, and in the second one, both the ABS and BGC spectra, and the concentration profiles of ABS and the non-absorbing solutes, were recovered by orthogonal projection approach (OPA) and alternating least squares (ALS). The OPA–ALS processing provided the deconvolved signals and the wavelengths required to implement the experimental and software-emulated NBDW procedures. A composite ABS spectrum and a mixed concentration profile of the non-absorbing solutes, that involves mutual ABS–BGC dilution effects are enclosed in the OPA–ALS straightforward solutions. The pure spectra and concentration profiles were finally retrieved by crossed orthogonalisation. For the NBDW procedures, the limits of detection ($S/N = 3$) for AES oligomers overlapped by 1500 $\mu g\,ml^{-1}$ ABS were of ca. 10 $\mu$M AES. Using decyl sulfate as internal standard, the relative standard deviation for AES in an ABS containing industrial sample was 4.5%. The procedures here described are useful to remove the interference produced by any absorbing solute when overlapped with indirectly detected solutes in both capillary electrophoresis (CE) and HPLC.


*Keywords:* Null-balance detection window; Multivariate deconvolution; Orthogonal projection; Indirect detection interferences; Alternating least squares; Alkyl ether sulfates; Alkyl benzene sulfonates; Ethoxylated alkyl sulfates

## 1. Introduction

Mixtures of several classes of surfactants, constituted by series of homologues and isomers, are usually found in manufactured products of the detergent and cosmetic industries. Judicious selection and careful optimisation of the separation and detection conditions have led to a number of HPLC [1–15] and capillary electrophoresis (CE) [9,10,16–31] methods, capable of resolving surfactant classes in their homologue and isomer constituents. Thus, absorbing ionic [9,10,17–19,25,27,28,31], absorbing non-ionic [10,16,22–24,29], and non-absorbing ionic surfactants [10,20,21,30] have been characterised and quantified by CE.

Alkyl benzene sulfonates (ABS), an important class of absorbing anionic surfactants, have been separated by using aqueous [32–34] and non-aqueous [18,25–27,31,35]

*Abbreviations:* ABS, alkyl benzene sulfonate; ACN, acetonitrile; AES, alkyl ether sulfate; ALS, alternating least squares; AQCA, anthraquinone-2-carboxylic acid; BGC, background chromophore; BGE, background electrolyte; DPA, dipentylamine; LOD, limit of detection; NBDW, null balance detection wavelength window; OPA, orthogonal projection approach; SDS, sodium dodecyl sulfate; TMBA, trimethoxy benzoic acid

* Corresponding author. Tel.: +34-963-543003; fax: +34-963-544436.
*E-mail address:* ramis@uv.es (G. Ramis-Ramos).

0021-9673/$ – see front matter © 2004 Elsevier B.V. All rights reserved.
doi:10.1016/j.chroma.2004.03.018

background electrolytes (BGEs), in some cases with both homologue and positional isomer resolution [25,31]. For the detection of non-absorbing analytes, a BGE containing a background chromophore (BGC) [5,36–38] is used. Thus, alkyl ether sulfates (AES) have been separated with oligomer resolution by HPLC with gradient elution and evaporative light scattering detection [5], and by CE with aqueous (with 40–50% acetonitrile, ACN) [20,21] and non-aqueous BGEs (ACN/MeOH mixtures) [20,30]. Numerous CE procedures for fatty acids have been also proposed [39–52].

However, to characterise and evaluate surfactant classes in the complex mixtures frequently found in cleaning products and toiletries still constitutes a challenging issue. Grob and Steiner [30] have reported the separation of the following mixtures: (a) alkyl sulfates and secondary alkane sulfonates, (b) alkyl sulfates and AES, (c) alkyl sulfates and ABS and (d) alkyl sulfates, secondary alkane sulfonates, AES and ABS, but with extensive overlapping of the AES and ABS peaks. The pair of classes AES–ABS was partially resolved using 80% ACN and 0.001% polybrene in the presence of 2-naphthalene sulfonic acid as BGC [30].

Owing to the low price and high cleaning power of ABS, the mixtures AES–ABS, AES–ABS-fatty acids and other combinations of anionic surfactants containing ABS are most frequently found in the formulations. In a previous work, we reported a procedure to analyse mixtures of AES and carboxylic acids [53]. Unfortunately in the recommended BGEs, the ABS homologues were found to appear just in the middle of the migration time region of the AES oligomers, thus causing severe interference. Attempts to modify the BGEs recommended for AES and carboxylic acid mixtures, thus to increase the separation between the AES and ABS classes, led to a decrease of the resolution between the AES oligomers, as well as that of the lighter carboxylic acids with respect to the heavier AES oligomers. Further, the need of maintaining the sensitivity of indirect detection severely conditioned the BGE composition.

Therefore, three quite different approaches, all them based on the use of a diode array detector, were developed in this work to remove the interference of ABS from the fatty acid and AES electropherograms. First, the contribution of the absorbing ABS interference to the signal was cancelled via selection of the appropriate BGC and wavelength range for the detection window, thus to yield suitable selective electropherograms for the non-absorbing solutes. Besides, two multivariate approaches, capable of taking full advantage out of the two-way (migration time–wavelength) data matrix provided by the diode array detector, were also developed. Several data analysis approaches based on either spectral comparisons or in the use of latent variables have thrived up to become the most valuable tools nowadays available to assess peak purity and to deconvolve overlapped signals [54]. We have used the comparative method known as orthogonal projection approach (OPA) [55] to find out the most dissimilar spectra contained in the data matrix in order to be used as initial estimates for a subsequent alternating least squares (ALS) [56,57] refining step. Both OPA and the OPA–ALS procedures were found to be also useful to locate cancelling detection wavelength windows of known and unknown absorbing interferences. The three procedures here described can be universally applied to remove overlapped absorbing interferences when non-absorbing solutes are indirectly monitored after CE or HPLC separation.

## 2. Materials and methods

### 2.1. Instrumentation and working conditions

An HP 8453 diode array spectrophotometer provided with a standard 1 cm quartz cell, an HP$^{3D}$ CE system (Agilent Technologies, Waldbronn, Germany), and fused-silica capillaries (Composite Metal Services Ltd., Ilkley, UK) of 80.5 cm (72 cm effective length) × 50 μm i.d. (363 μm o.d.), were used. Concerning the subject of this work, it is worth to indicate that the CE instrument was able to simultaneously monitoring up to five detection wavelength windows of different sizes located at assorted wavelengths, and that, using the corresponding software option, a full spectrum every 0.2 s can be also stored during the experimental runs. These spectra were constituted by 40 evenly spaced absorbances between 220 and 300 nm (spectral resolution, 2 nm). Separations were performed at 45 °C under +20 kV.

New capillaries were treated with 1 and 0.1 M NaOH and water at 60 °C (10 min each). Daily before use, the capillary was rinsed with 0.1 M NaOH (20 min), water (10 min) and the running buffer (10 min) at 45 °C. Between runs, it was conditioned with 0.1 M NaOH (10 min), water (2 min) and the running buffer (8 min). After each working session, it was flushed with water for 10 min. Before injection, all solutions were filtered through a 0.45 μm pore-size nylon membrane (Albet, Germany). Hydrodynamic injection (5 kPa × 3 s) was used. An 80 nm wide and 380 nm centred reference window was used in all cases with the several detection wavelength windows studied along the work. When working in the indirect detection mode, the measuring and reference wavelengths were interchanged thus to obtain positive peaks.

### 2.2. Reagents and solutions

Carboxylic acids and ABS homologues were named after the number of carbon atoms in the alkyl chain, with a preceding Φ to account for the ABS phenyl sulfonic group and lack of the carboxylic group; for instance, C12 is dodecanoic acid, but ΦC12 is dodecylbenzene sulfonic acid; C12E2 represents an AES oligomer with an alkyl chain of 12 carbon atoms, plus two ethylene oxide groups and the sulfate group at the end.

Acetonitrile (ACN), dioxane (Scharlab, Barcelona, Spain), 3,4,5-trimethoxybenzoic acid (TMBA), anthraquinone-2-carboxylic acid (AQCA), dipentylamine (DPA), acetic (C2), capric (C10), lauric (C12), myristic (C14) and

palmitic (C16) acids (used to help in peak identification) [53], sodium decyl sulfate (C10E0, used as internal standard in calibration), sodium dodecyl sulfate (SDS or C12E0), sodium tetradecyl sulfate (C14E0) and sodium hexadecyl sulfate (C16E0) (Sigma–Aldrich, Steinheim, Germany, and Fluka, Buchs, Switzerland) were used. A 27% (w/w) aqueous AES solution (supplied by Químicas Oro S.A., Sant Antoni de Benaixever, Spain), 4-dodecylbenzenesulfonic acid (technical mixture of ABS homologues, ~90% purity, Fluka), with a declared average molecular weight of $\bar{M} = 326.49\,\mathrm{g\,mol^{-1}}$, and deionised water (Barnstead deioniser, Sybron, Boston, MA) were also used.

A $10\,\mathrm{mg\,ml^{-1}}$ ABS and AES stock solutions were prepared in water (AES dilution was made according to its declared concentration). A mixture containing C10–C16 ($200\,\mu\mathrm{g\,ml^{-1}}$ each, solved in 50:50 methanol/water, (v/v)) and a $1000\,\mu\mathrm{g\,ml^{-1}}$ C10E0 (internal standard) solution in water were also prepared. These solutions were adjusted dropwise to pH 10 with 1 and 0.1 M NaOH. The BGE contained 5 mM AQCA, 7 mM DPA, 85% ACN, 5% dioxane and water [53].

## 3. Results and discussion

### 3.1. Cancellation of the ABS interference by selection of the BGC and the detection wavelength window

Electropherograms of ABS and AES solutions, obtained by indirect detection at 260 nm (inverted negative absorbance peaks), are shown in Fig. 1. At this wavelength AQCA has an absorption maximum and ABS does not absorb, which implies maximum sensitivity for the indirect detection of both ABS (trace A) and the non-absorbing AES and fatty acids (trace B). The ABS electropherogram showed four large peaks that roughly corresponded to the ΦC10–ΦC13 homologues, although with some overlapping of the isomers of adjacent homologues [31]. As deduced by comparing traces A and B, ABS and AES peaks seriously overlapped. An electropherogram for ABS, free of the interference of AES, can simply be obtained by monitoring at the wavelength of maximal ABS absorption (i.e. 225 nm) in the direct detection mode (positive absorbance peaks); however, detection of non-absorbing solutes, as AES and fatty acids, is limited to the indirect mode, thus, any co-migrating (or co-eluting) aborbing solute will interfere. As demonstrated next in this section, the indirect detection of AES, without the interference of ABS is possible if an adequate spectral window for detection is used. Acquisition of the two-way data matrix is not required; however, as shown later in Sections 3.2 and 3.3, the detection of both the non-absorbing solutes and ABS in a single injection is also possible by using information stored that matrix.

In indirect detection, the signals are produced by substitution of the BGC probe ions by those of the solutes. Thus for univalent anions and using the indirect detection mode, a solute having exactly the same molar absorptivity than that of the probe ions cannot be detected. For a probe ion with a charge $z_p$ which is replaced by a solute with a charge $z_a$, the generalised undetectability condition is:

$$z_p\varepsilon_p = z_a\varepsilon_a \quad (1)$$

where $\varepsilon_p$ and $\varepsilon_a$ are the molar absorptivities of the probe and the solute ions, respectively. Fig. 2 shows the absorption spectra of TMBA, AQCA and ABS, where the *Y*-axis has been expressed in molar absorptivity units. The spectra were recorded in the HP 8453 spectrophotometer with care of not surpassing an absorbance of 1.5, thus to avoid distortion by stray radiation, then, the molar absorptivities were calculated by dividing the absorbances by the respective

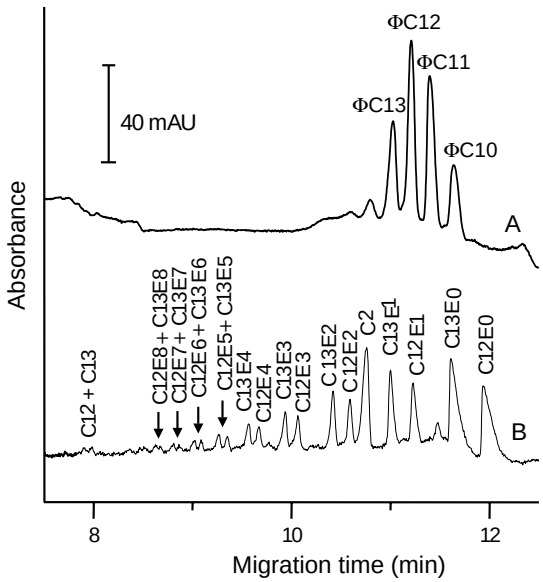


Fig. 1. Electropherograms of $1500\,\mu\mathrm{g\,ml^{-1}}$ solutions of ABS (A) and AES (B) obtained by indirect monitoring at 260 nm with a 10 nm wide window; EOFs at ca. 6.2 and 5.9 min, respectively.

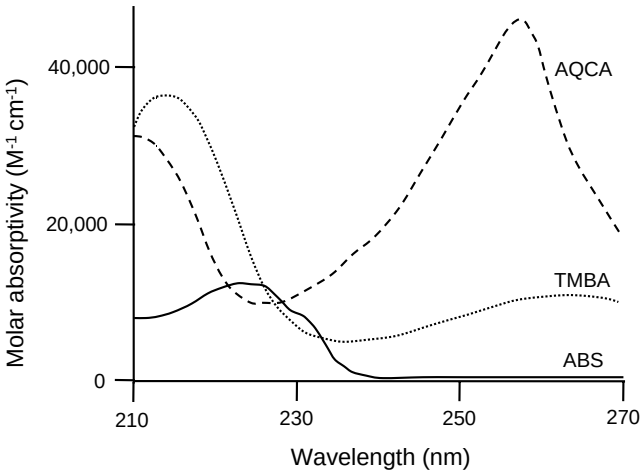


Fig. 2. Absorption spectra of TMBA, AQCA and ABS divided by the respective molar concentrations; the spectra were recorded at 25 μM for TMBA and AQCA, and 130 μM for ABS.

molar concentrations. For ABS, the average molar concentration given by the manufacturer was used. ABS is in fact a mixture of species, but as an approximation, it can be assumed that all of them have the same absorption spectrum; this seems reasonable, since the spectrum of each oligomer depends mainly on the benzene sulfonate group rather than on the length differences between the alkyl chains. Finally, since these are monovalent anions, the spectra of Fig. 2 are not modified by multiplying the *Y*-axis by the respective charges. Fig. 2 revealed the presence of two points per solute where Eq. (1) was fulfilled, i.e. 221 and 227 nm for AQCA and 226 and 232 nm for TMBA. At these wavelengths, the respective absorptivity spectra cross over the ABS absorptivity spectrum.

However, a window extended over a range of wavelengths instead of a single wavelength is required to implement detection properly, thus to achieve adequate signal-to-noise ratios. In indirect detection, and at any wavelength along the detection window, a solute having a molar absorptivity lower than that of the BGC contributes to increase the signal in the indirect detection mode, whereas this signal decreases when the molar absorptivity of the solute is higher than that of the BGC. Thus, for an absorbing solute to be undetectable when a $\Delta\lambda$-wide detection window centred at the *j*-wavelength is used, the following condition should be met:

$$S = z_p \sum_{j=-\Delta\lambda/2}^{j=+\Delta\lambda/2} \varepsilon_{p,j} - z_a \sum_{j=-\Delta\lambda/2}^{j=+\Delta\lambda/2} \varepsilon_{a,j} = 0 \quad (2)$$

According to Eq. (2), around each point satisfying Eq. (1), a family of charge-absorptivity null-balance detection windows (NBDWs), where the sum of the positive and negative contributions to the signal cancel each other, can be defined by varying $\Delta\lambda$. Any addressed absorbing solute should be undetectable if a detection wavelength window fulfilling Eq. (2) is used. As can be also deduced from Eq. (2), an NBDW does not exist for solutes having molar absorptivities lower than those of the BGC at all wavelengths; however, as discussed later in Section 3.3, cases like this one can be successfully handled by using multivariate approaches.

In Fig. 3, values of *S*, calculated according to Eq. (2) for the AQCA–ABS and TMBA–ABS pairs, are plotted against the central wavelength of a series of windows of increasing widths. On this plot, the crossing points of the curves with the $S = 0$ line indicate the wavelengths where NBDWs of a given width exist. The plot also shows that, for each BGC–solute pair, as $\Delta\lambda$ increases, the two NBDWs (centred around the two wavelengths where Eq. (1) holds) merge to a single window of maximal width. For a given BGC–solute pair, an NBDW is not possible anymore beyond that maximal width. Eq. (2) predicted a maximal NBDW width of 9 nm for both the AQCA–ABS and TMBA–ABS pairs; the centres of the maximal NBDWs were predicted at 225.0 and 229.5 nm, respectively.

Since observation windows within the 10–20 nm range are most frequently used in CE, and since smaller windows would have yielded lower signal to noise ratios, the maximal 9 nm width NBDWs were selected. The optimal NBDWs for AQCA and TMBA in Fig. 3 were centred at wavelengths where the respective molar absorptivities are of ca. 10,000 and 7000 $M^{-1}\,cm^{-1}$; thus, the sensitivity of indirect detection using the corresponding optimal window for AQCA should be higher than using the optimal TMBA window, hence the former was finally selected as BGC.

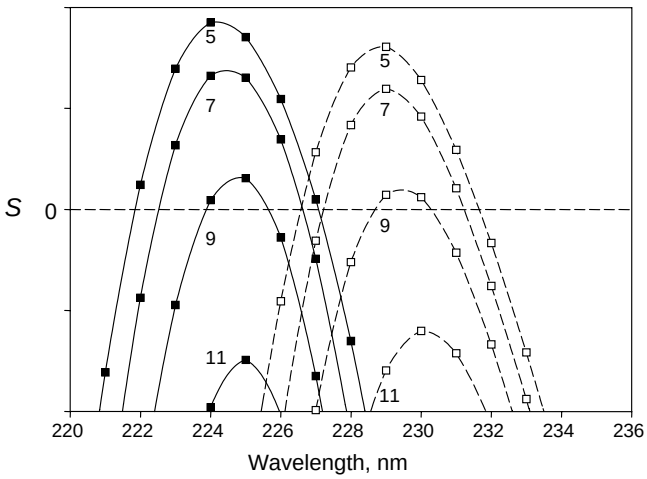


Fig. 3. Values of *S* according to Eq. (2) plotted against the wavelength at the centre of the observation window; the numbers at the lines indicate window widths in nm, the continuous lines are data for the AQCA–ABS pair, and the dashed lines correspond to the TMBA–ABS pair.

Figs. 2 and 3 were calculated using data obtained with the HP 8453 spectrophotometer; however, this instrument may slightly differ from the CE detector in terms of slit width, wavelength calibration and maybe also in the way the on-line acquired data are processed. Further, attempts of recording the ABS and AQCA spectra using the CE instrument revealed significant differences along the molar absorptivity scale regarding the HP 8453 data. Thus, the width and central wavelength of the maximal NBDW for the AQCA–ABS pair that were predicted from the HP 8453 spectra by using Eq. (2), were also experimentally optimised using the CE detector. For this purpose, the width and central wavelength of the maximal NBDW found above were used as a first approximation, thus to record electropherograms of an ABS solution using detection windows of increasing widths (from 5 to 13 nm) whose central wavelength was moved from 223 up to 231 nm. The series for the 9 nm wide windows is shown in Fig. 4.

The best NBDW was obtained for a 9 nm wide window (as expected), but the best location of the window centre was 227 nm (instead of the value obtained with the HP 8453 spectrophotomer, 224 nm). As shown in Fig. 4, small negative peaks for the ΦC13, ΦC12 and ΦC10 homologues, and a small positive peak for ΦC11, were still observed with the optimal NBDW. These residual peaks could be explained as due to the sensitivity drift associated to the increase of electrophoretic mobility along the time axis, although small

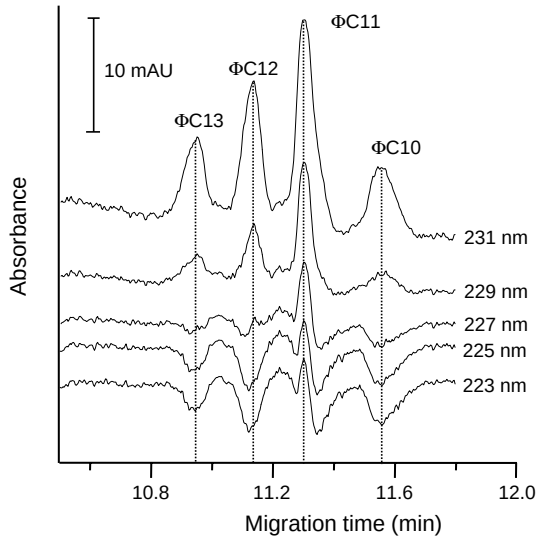


Fig. 4. Electropherograms of a 1500 μg ml$^{-1}$ ABS solution obtained by indirect monitoring with a 9 nm wide window centred at the wavelengths indicated at the traces; EOF at 6.1 min.

differences between the molar absorptivities of the ABS homologues (may be due to the different isomeric distribution) could also contribute.

The relative values of the signals still left at the migration times of the four homologues were estimated as follows. First, the ABS signal in the indirect mode was recorded with a 9 nm wide window centred at the wavelength of maximum absorption of AQCA, 260 nm, where ABS does not absorb. Then, this signal was multiplied by the ratio of AQCA absorptivities at 227 and 260 nm to obtain the almost matched peak heights that would have been shown by both ABS and AQCA in the respective direct and indirect detection modes at 227 nm if mutual signal cancellation would have not been produced. According to these peak heights, the residual absorbances observed in Fig. 4 for the 227 nm trace amounted to a 1.2, 0.7, −4.5 and 2.6% for the ΦC13, ΦC12, ΦC11 and ΦC10 homologues, respectively. Therefore, for a mixture of homologues (as occurs with ABS) rather than for a single solute, a perfect signal cancellation can be achieved for the sum of the homologues, small residual peaks remaining for the individual homologues. A perfect signal cancellation at all the migration times seems impossible to be accomplished by using a single detection wavelength window. The simultaneous use of several NBDWs, tuned to the requirements of the successive homologues, is feasible, but it was not assayed in this work. Systematic errors in the evaluation of the overlapped non-absorbing solutes by indirect detection were left as a consequence of adopting a single common NBDW; however, as these errors were both small (attention should be paid to the *Y*-axis expansion in Fig. 4) and non-dependent on the AES concentration, they were assumed to be significant only at very low AES concentrations.

Electropherograms of an ABS–AES mixture obtained by using two different detection wavelength windows are shown

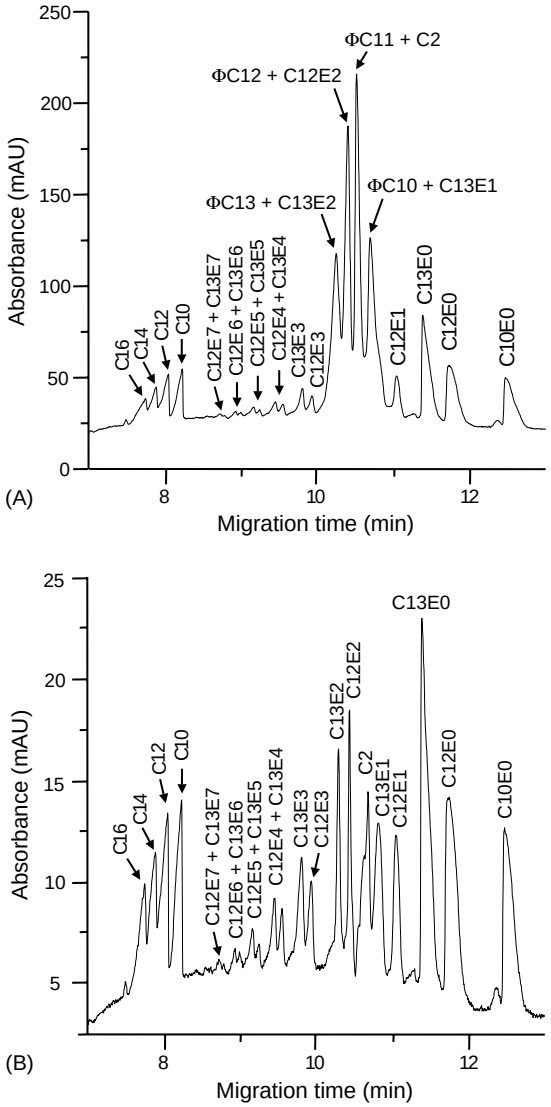


Fig. 5. Electropherograms obtained with a single injection and simultaneous monitoring at two detection wavelength windows of a mixture containing 1250 μg ml$^{-1}$ of each ABS and AES, C10–C16 (50 μg ml$^{-1}$ each) and 100 μg ml$^{-1}$ C10E0 (internal standard); monitoring was performed with a 10 nm wide and 260 nm centred window (A) and with the optimal NBDW (9 nm wide and 227 nm centred) (B); EOF at 5.9 min.

in Fig. 5. Extensive peak overlapping was observed by monitoring at the wavelength of maximal sensitivity for indirect detection with AQCA, 260 nm (trace A). In contrast, monitoring with the maximal NBDW (9 nm wide and 227 nm centred) yielded well resolved AES peaks essentially free from the ABS interference (trace B). The resolved peak of acetate (C2, a common impurity of AES) was also observed on trace B.

The lower signal to noise ratio of Fig. 5, trace B, with respect to Fig. 1, trace B, was mainly due to the reduction of the molar absorptivity of the BGC at 227 nm (10,000 M$^{-1}$ cm$^{-1}$) with respect to its value at the wavelength of the maximum, 260 nm (45,800 M$^{-1}$ cm$^{-1}$) (although the concentration of AES was also slightly lower in

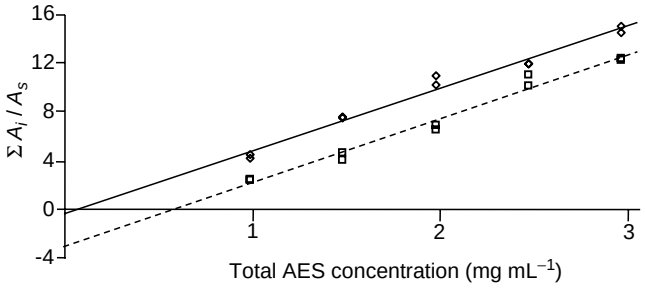


Fig. 6. Regression straight-lines obtained with the optimal NBDW (9 nm wide and 227 nm centred) (◇) and using a 10 nm wide and 222 nm centred window (□); sums of the corrected areas of the C10E0–C13E8 peaks divided by the corrected area of the internal standard peak are plotted on the *Y*-axis.

Fig. 5). The signal to noise ratio to be reached by using the proposed monitoring procedure is thus limited by both the width and location of the maximal NBDW and the average molar absorptivity of the BGC at that NBDW. Fortunately for the AQCA–ABS pair, the maximal NBDW had a reasonable width (9 nm), the wavelength of the window centre was not too low (227 nm), and was located in the vicinity of the wavelength of the ABS absorption maximum, which is an optimum case. Thus, in addition to the electrophoretic factors, the spectra of both the BGC and the addressed interfering absorbing solute should be considered in the selection of the BGC to define an optimal NBDW.

The calibration straight-line of Fig. 6 (continuous line) was obtained by using the optimal NBDW (9 nm wide and 227 nm centred), by measuring the corrected areas of the C10E0–C13E7 peaks, and by dividing its sum by the corrected area of the peak of the internal standard. As shown in the same figure, and as revealed by the negative intercept, a calibration straight-line obtained with an unbalanced window (10 nm wide and 222 nm centred, dashed line), was affected by a large systematic constant error due to the ABS interference.

### 3.2. Emulating the NBDW procedure by software

In the experiments of Fig. 5 and in those used to construct Fig. 6, each electropherogram was both recorded on the monitor screen (and file printed) and stored as an $m \times n$ data matrix, **X**, where each row contained a full spectrum (the absorbance at $n$ wavelengths) at a specific migration time. Along the wavelength scale and for the non-absorbing solutes, the sensitivity roughly followed the AQCA absorptivity, but for ABS the sensitivity depended on the difference between the own and the AQCA spectra. Since the ABS and AQCA spectra are rather different, it can be expected the two-way electropherograms to contain enough information for the underlying electropherograms of the non-absorbing solutes and ABS to be separately retrieved. This can be done either by using multivariate deconvolution techniques, which are discussed in Section 3.3, or in a simpler way, by software emulation of the above explained procedure based on an NBDW, thus mimicking what was done above with series of moving windows of increasing sizes.

First, the information stored in the **X** matrix was used to examine the influence of the location and size of the detection wavelength window on the background noise. For this purpose, time regions showing no peaks were used, and the standard deviation of the background was averaged along series of wavelength windows centred at increasing wavelengths and having increasing sizes. The background noise was observe to increase significantly either when $\Delta\lambda < 3$ nm and for windows centred at wavelengths below 220 nm, thus, these values were avoided in the studies that followed.

Exploration of **X** in order to find out an optimal NDBW can be certainly done in several ways, but the procedure explained next was found to perform fairly well. First, the crossing points of Fig. 2 (where Eq. (1) holds) should be located on **X**. This can be achieved by OPA–ALS deconvolution (explained in Section 3.3), or in a more simple way by applying purity assays to the transpose of the data matrix, $\mathbf{X}^{\mathrm{T}}$ (for instance, using OPA). Using these two procedures, the points where Eq. (1) holds were located at 220.5 and 228.5 nm. The profile at 228.5 nm was taken as a reference, thus this will be called next the reference wavelength. Second, to find out the software-emulated optimal NBDW, the concentration profile at 228.5 nm was compared with the concentration profile averaged within the wavelength window being tested. The comparison was made attending at a peak location which was free from the ABS contribution (the F-time), and at the $n = 4$ ABS peak locations, that are the migration times bearing serious interference (the I-times). A purity assay can be used to locate suitable F- and I-times; for this purpose, we also applied OPA (see Section 3.3). The following difference was then calculated:

$$d_{\Delta\lambda} = n(p_{\mathrm{F},\Delta\lambda} - p_{\mathrm{F,R}}) - \sum(p_{\mathrm{I},\Delta\lambda} - p_{\mathrm{I,R}}) \quad (3)$$

where $\Delta\lambda$ is the width of the tested wavelength window, $p_{\mathrm{F},\Delta\lambda}$ and $p_{\mathrm{I},\Delta\lambda}$ denotes the average signal at the F- and I-times within the window, and $p_{\mathrm{F,R}}$ and $p_{\mathrm{I,R}}$ are the corresponding signals for the reference wavelength, the sum of the second parenthesis being extended to the $n = 4$ ABS peaks. Since $d_{\Delta\lambda}$ is proportional to the sum of the ABS peak residuals, windows where the interference is fully cancelled should yield zero $d_{\Delta\lambda}$ values.

An initial 8 nm wide window, centred at 224.5 nm (the middle point between the two software-located cancellation points, 220.5 and 228.5 nm) was first considered, and 2 nm increments (the resolution along the rows of **X**) were successively added to the window ends. The 224.5 nm centred window giving the lowest $d_{\Delta\lambda}$ was retained. The process was repeated using windows centred at neighbouring wavelengths, until a further reduction of $d_{\Delta\lambda}$ was no longer possible. A contour plot of $d_{\Delta\lambda}$ showed a similar pattern as that calculated in Fig. 3 for AQCA (continuous lines) using Eq. (2). A 14 nm wide and 224.5 nm centred optimal NBDW resulted. The differences with respect to the optimal

NBDW deduced above (9 nm wide and 227 nm centred) could be due to a better spotting of the optimum along the two variables involved, i.e. window width and centre. The electropherograms of ABS obtained by regression of both its pure spectrum and that of the BGC on **X**, and those of the non-absorbing solutes extracted from **X** by averaging the electropherograms within this emulated maximal NBDW, were closely similar to those shown in Fig. 1, traces A and B, respectively. Further, the electropherograms of AES obtained by the experimental (Fig. 5, part B) and emulated NBDW procedures were closely similar.

Information provided by the previously recorded absorption spectra of both the BGC and the interference was used in Section 3.1 to locate the experimental maximal NBDW, which was then further optimised using two series of electropherograms recorded at different detection wavelength windows. In this section, the systematic examination of **X** using OPA has resulted in an emulated maximal NBDW without previous knowledge about the spectrum of the interference, and using a single experimental run, without requiring further optimisation. A more general approach, based on the OPA–ALS algorithm, and also able to rapidly spot an NBDW using a single **X** matrix, is outlined in the next section.

### 3.3. Full multivariate deconvolution by OPA–ALS

The AQCA–ABS pair is, in fact, a particular case of a more general problem, namely the resolution of the overlapped signal of indirectly detected solutes by an absorbing interference in both CE and HPLC. In this concern, the procedures described above rely on two particularly favourable circumstances, i.e. for the experimental NBDW procedure, reliable spectra of both the interference and the BGC should be available, and with both the experimental and software-emulated NBDW procedures, a suitable maximal NBDW should exist. However, procedures not making use of these favourable features should be developed for the general case to be addressed.

The different ways this can be done for both the particular and general cases are outlined in the flow diagram of Fig. 7. If reliable spectra of both the BGC and the interference are available (the spectrum and nature of the latter could be unknown), and at least if an NBDW exists, then at least one of the NBDW procedures of above can be used. Otherwise, multivariate curve resolution—ALS can be applied to achieve full resolution of the contributions of the non-absorbing and absorbing solutes. Two steps are involved in the calculation process. The first one is the so called purity assay, where the number of species present in **X** having different spectra (i.e. one or more than one interfering absorbing species and the BGC) is determined. The purity assay also provides estimates of those spectra. In the second step, the tentative spectra are used to establish both spectra with an improved reliability and the concentration profiles, from which isolated electropherograms of the absorbing and non-absorbing solutes can be finally calculated.

Several purity assays, based or not on latent variables, have been proposed [54]. In this work, OPA, whose performance has been widely demonstrated in providing initial estimates for deconvolving overlapped peaks detected in the direct absorbance mode in HPLC [54,55], was selected. In OPA, each spectrum contained in the $m \times n$ **X** data matrix is systematically contrasted with a collection of normalised reference spectra, in order to find out which one of the $m$ spectra is less compatible with those in the collection. The core of the method is the assessment of dissimilarity, which is a property that establishes the orthogonality level in a set of spectra. Thus, for instance, if a given target spectrum is extracted from **X**, the dissimilarity will be calculated as follows: the spectrum is first normalised and arranged with the $r$ normalised reference spectra in the collection to obtain an $(r+1) \times n$ matrix, **Y**. The dissimilarity is then obtained by:

$$\mathrm{dis}(\mathbf{Y}) = \mathrm{Det}(\mathbf{Y}^{\mathrm{T}}\mathbf{Y}) \tag{4}$$

This comparison is then extended to all spectra contained in **X**, and the dis(**Y**) values are plotted versus the migration (or elution) time, yielding what is called a dissimilarity plot, whose maximal value denotes the most incompatible spectrum in **X** with those in the collection. The process usually starts setting as **Y** the mean spectrum of **X**. In the next iteration, the spectrum associated to the migration time where the dissimilarity plot shows the maximal value is substituted by the old spectrum in **Y**. The process follows by successively adjoining the most dissimilar spectrum found in **X** to **Y**, and by re-plotting the dissimilarities up to only noise remains.

OPA finds out both the number of solutes and estimates of their purest spectra. However, one should note that usually the spectra yielded by OPA are just tentative solutions that require further refinement. This can be conveniently achieved by ALS, a multivariate technique that decomposes bilinear (or tri-linear) matrices in concentration and absorbance profiles by alternating two least squares regressions, i.e. the spectral profiles on **X** to obtain the concentration profiles, **c**, and the concentration profiles on **X** to obtain the spectral profiles, **s**, repeating this process alternatively. This can be expressed as:

$$\mathbf{c} = \mathbf{X} \cdot (\mathbf{s}^{\mathrm{T}} \cdot \mathbf{s})^{-1} \cdot \mathbf{s}^{\mathrm{T}} \tag{5}$$

$$\mathbf{s} = (\mathbf{c}^{\mathrm{T}} \cdot \mathbf{c})^{-1} \cdot \mathbf{c}^{\mathrm{T}} \cdot \mathbf{X} \tag{6}$$

If no further operation is applied, the cycle will end yielding the same initial spectral (or concentration) profile used to start the iteration, except in noise, which will be amplified. This later would make the process to diverge, and no benefit would be obtained. The way how ALS achieves convergence yielding successful final solutions is the imposition of constraints to the intermediate solutions. Thus, after each regression, some constraints are applied to guarantee that the process will converge in solutions with physicochemical meaning. For instance, negative peaks are not allowed by

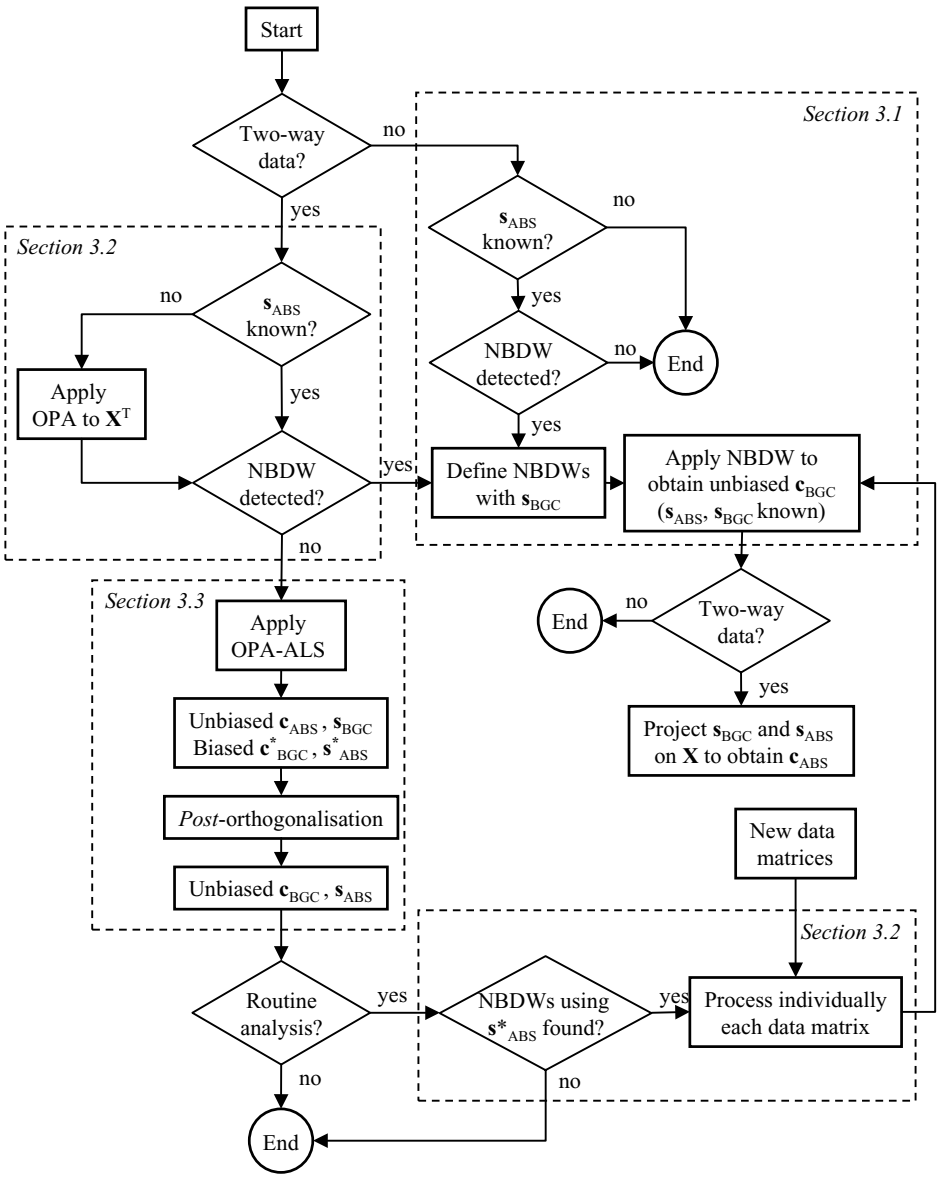


Fig. 7. Flow chart of the general non absorbing–absorbing two-way deconvolution problem, showing the main splitting points and the solutions investigated in this work; **X** is the two-way data matrix, **s** and **c** denote vectors containing a spectrum and a concentration profile, respectively, and the asterisks indicate either a composite spectrum or a composite concentration profile.

the positivity constraint, and secondary maxima per solute are either prevented by the unimodality constraint. These and other constraints have been used in HPLC [58,59] and CE [57] to deal with the deconvolution of directly detected overlapped chromophores.

In the case of concern, after baseline subtraction, only positive multimodal signals are expected for the pure ABS contribution. Accordingly, the no-negativity constraint should be applied to its concentration profile. However, a composite spectrum, which will be a linear combination of the ABS and BGC spectra will be obtained. Therefore, no constraint concerning the signal sign can be applied to the ABS spectrum. Consequently, ALS will originate a good estimation of the ABS concentration profile but a fake ABS spectrum.

On the other hand, the BGC signal gathers dilution effects due to both the non absorbing and the absorbing solutes. Since dilution effects on the BGC are expected to provide negative signals, a no-positivity constraint should be applied to the BGC multimodal concentration profile. Note that the ABS true signal is being considered as split in two parts, i.e. a dilution and an absorption contributions.

Finally, the no-negativity constraint can also be applied to the BGC spectrum. In addition, there are selective migration time regions where the peaks of the non-absorbing species are free from the ABS interference. Therefore, it is possible to impose a selectivity constraint within the selective time windows, where any contribution of the absent species to the signal is zeroed.

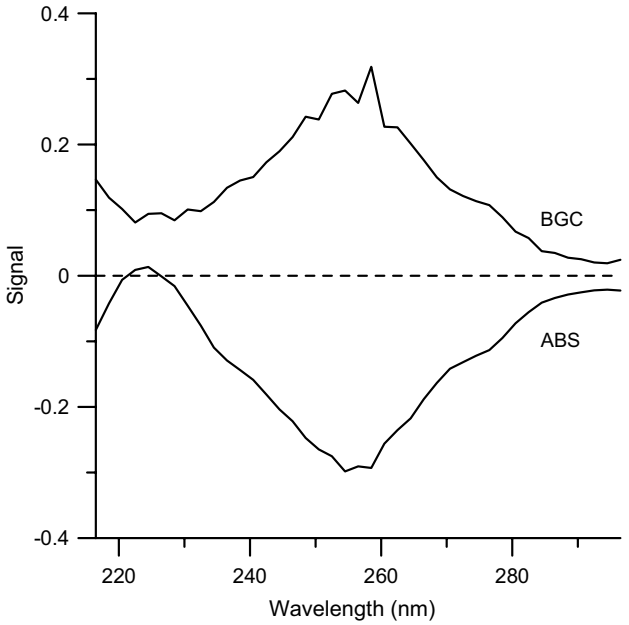


Fig. 8. Raw spectral profiles ($\mathbf{s}_{BGC}$ and $\mathbf{s}^*_{ABS}$) found by ALS before orthogonalisation. The spectra are normalised, and the signs are arbitrary. The existence of points where Eq. (1) holds is evidenced by the wavelengths where $\mathbf{s}^*_{ABS}$ equals zero.

The ALS algorithm used in this work, implemented with these four constraints, and using as initial estimates the spectra provided by OPA, converged within a few iterations. Among the information retrieved, the pure BGC and combined ABS spectra will be next considered. As indicated above, the ABS spectrum found is a linear combination of the ABS and BGC pure spectra. As shown in Fig. 8, null-balance points (if exist) are evidenced at those wavelengths where this combined ABS spectrum equals zero. At these wavelengths (on the figure, 220.5 and 228.5 nm), the dilution effects produced by ABS on the BGC signal equal its own absorption. If exist, location of these points by the OPA–ALS algorithms allows the application of the faster and simpler NBDW procedures explained above to other samples that could be affected by the same interfering absorbing solute. Used in this way, ALS becomes a useful tool to look for NBDWs of unknown interferences. This possibility was also included in the flow chart of Fig. 7.

As shown next, to fully deconvolute the electropherograms of the absorbing interference and the non-absorbing solutes by OPA–ALS, further treatment of the solutions originally provided by ALS is required. ALS decomposes the data matrix as follows:

$$\mathbf{X} = \mathbf{X}_{BGC} + \mathbf{X}_{ABS} + \mathbf{E} = \mathbf{c}^*_{BGC} \cdot \mathbf{s}_{BGC} + \mathbf{c}_{ABS} \cdot \mathbf{s}^*_{ABS} + \mathbf{E} \quad (7)$$

where $\mathbf{X}_{BGC}$ and $\mathbf{X}_{ABS}$ are the contributions of the BGC and the absorbing interference (ABS in the case of concern) to the two-way signal, and $\mathbf{E}$ is the residual matrix. Eq. (7) also expresses that ALS convergence leads to the right spectrum for BGC, $\mathbf{s}_{BGC}$, but the retrieved concentration profile, $\mathbf{c}^*_{BGC}$, is composite (the asterisk indicates that this is a biased concentration profile). For ABS the situation is the opposite, i.e. ALS yields a good estimation of the ABS concentration profile, $\mathbf{c}_{ABS}$, but a biased spectrum, $\mathbf{s}^*_{ABS}$.

Either the true BGC concentration profile or the pure ABS spectrum can be retrieved by orthogonalisation of $\mathbf{c}^*_{BGC}$ or $\mathbf{s}^*_{ABS}$, respectively. Orthogonalisation of $\mathbf{X}_{BGC}$ consists in the suppression of the spurious contribution associated to ABS in $\mathbf{X}_{BGC}$, which can be done by using the known unbiased information about the interference, which is its concentration profile, $\mathbf{c}_{ABS}$. Analogously, orthogonalisation of $\mathbf{X}_{ABS}$ consists in the suppression of the contribution associated to the BGC in $\mathbf{X}_{ABS}$, by using its pure spectrum, $\mathbf{s}_{BGC}$.

Orthogonalisation of $\mathbf{X}_{BGC}$ is done first by projecting the ABS concentration profile on $\mathbf{X}_{BGC}$; the fake spectrum obtained in this way is used to reconstruct the dilution contribution of the ABS in the BGC, which is then subtracted from the original $\mathbf{X}_{BGC}$ matrix:

$$\mathbf{X}_{cBGC} = \mathbf{X}_{BGC} - [\mathbf{c}_{ABS} \cdot (\mathbf{c}^T_{ABS} \cdot \mathbf{c}_{ABS})^{-1} \cdot \mathbf{c}^T_{ABS}] \cdot \mathbf{X}_{BGC} \quad (8)$$

where $\mathbf{X}_{cBGC}$ is the corrected $\mathbf{X}_{BGC}$ matrix, and the brackets contain the orthogonal projection operator of $\mathbf{c}_{ABS}$. Finally, the corrected concentration profile for AES will be obtained by projecting its spectrum on the corrected data matrix:

$$\mathbf{c}_{BGC} = \mathbf{X}_{cBGC} \cdot (\mathbf{s}^T_{BGC} \cdot \mathbf{s}_{BGC})^{-1} \cdot \mathbf{s}^T_{BGC} \quad (9)$$

Similarly, the true spectrum of the absorbing interference can be also obtained by:

$$\mathbf{X}_{cABS} = \mathbf{X}_{ABS} - [\mathbf{X}_{ABS} \cdot (\mathbf{s}^T_{BGC} \cdot \mathbf{s}_{BGC})^{-1} \cdot \mathbf{s}^T_{BGC}] \cdot \mathbf{s}_{BGC} \quad (10)$$

$$\mathbf{s}_{ABS} = (\mathbf{c}^T_{ABS} \cdot \mathbf{c}_{ABS})^{-1} \cdot \mathbf{c}^T_{ABS} \cdot \mathbf{X}_{cABS} \quad (11)$$

Orthogonalisation of $\mathbf{X}_{BGC}$ and $\mathbf{X}_{ABS}$ can be done a priori (within the ALS iterations) or a posteriori (after convergence). We selected the latter alternative, since the process converged readily, yielding in addition the wavelengths at which Eq. (1) holds (if they exist). A priori orthogonalisation should be the method of choice if no selective migration time (or spectral) window exists for either the interference or the BGC.

The OPA–ALS procedure was applied to the $\mathbf{X}$ matrixes of the ABS–AES mixtures used to construct the calibration straight-lines of Fig. 6. The concentration–time profiles of ABS were satisfactorily reconstructed, but distortions in the time profiles of the non-absorbing solutes were observed within the time region where ABS was present. It should be noted that the baseline correction is particularly troublesome in the case of concern, owing to the many ABS peaks that overlap peaks of non absorbing solutes along a wide migration time region; in this case, the baseline should be corrected by modelling point subsets that are too distant each

other. This also highlights the robustness of the NBDW procedures of above against baseline fluctuations, since baseline corrections are not required. However, as shown in the next section, the performance of the OPA–ALS procedure can be improved by applying additional baseline corrections.

### 3.4. Limits of detection and application to industrial samples

The limits of detection (LOD) for the AES oligomers that were and were not overlapped by ABS were estimated as follows. First, the bandwidth of the baseline of the electropherograms of mixtures containing 1500 μg ml$^{-1}$ ABS and 2000 μg ml$^{-1}$ AES was measured and taken as 5S.D. (S.D.: standard deviation), then, for individual oligomers, the LOD was calculated as 3S.D. divided by $h_i/[M_i]$, where $h_i$ and $[M_i]$ are the peak height and the molar concentration of the *i*th-oligomer. The latter was calculated as [53]:

$$M_i = \frac{A_i}{\sum A_i}\frac{C}{\bar{M}} \tag{12}$$

where $A_i$ is the area of the *i*th-oligomer peak, the sum is extended to all the AES oligomers showing significant peaks, $C$ is the AES concentration (g l$^{-1}$) of the pure form, and $\bar{M}$ is the average molecular weight of the AES standard, which was calculated as:

$$\bar{M} = \sum\left[\left(\frac{A_i}{\sum A_i}\right) M_i\right] \tag{13}$$

where $M_i$ is the molecular weight of the *i*th-oligomer, the sum being extended to all the oligomers, from C12E0 up to C13E7.

Provided that both the experimental and emulated NBDW procedures have led to a nearly full cancellation of the ABS contributions, the same LODs should be expected for both the interfered and non interfered peaks (as C13E2 and C13E0, respectively). Accordingly, the electropherograms obtained with the experimental NBDW procedure led to LODs of ca. 14 μM for both types of peaks, whereas the emulated NBDW procedure led to LODs of ca. 8 μM. In the same injections, and using a 10 nm wide window centred at the optimum wavelength for indirect detection with AQCA, 260 nm, the LOD for the non-overlapped AES oligomers was 6 μM.

The procedure was applied to identify and quantify the surfactants in household cleaners and toiletries containing both AES and ABS, and in some cases fatty acids were also present. The electropherograms of a soft cleaner for delicate clothes, obtained with a single injection by monitoring at the optimal wavelength for indirect detection with AQCA, and at the experimentally obtained maximal NBDW (9 nm wide and 227 nm centred), are shown in Fig. 9A and B, respectively. The corresponding isolated electropherogram of the non absorbing solutes, obtained by software emulation of the NBDW using **X** (not shown), was closely similar to that of Fig. 9B, however, a broad distortion in regions distant from those used to establish the baseline was observed for the electropherogram of the non-absorbing solutes obtained by OPA–ALS deconvolution. The usual pre-treatment based on diode-by-diode linear drift subtraction gave rise to deficient baseline corrections. Thus, further subtraction correction based on fitting skewed Gaussian functions to each diode, applied within baseline regions that were selected between consecutive peaks following the trend of the broad baseline distortion, was assayed. After orthogonalisation the heights of the reconstructed peaks were satisfactorily correlated with those measured in Fig. 9B.

Integration of the corrected peak areas of Fig. 9, trace B (sum of areas from C12E0 up to C14E7), and application of the calibration curve of Fig. 6, led to 2430 μg ml$^{-1}$ AES,

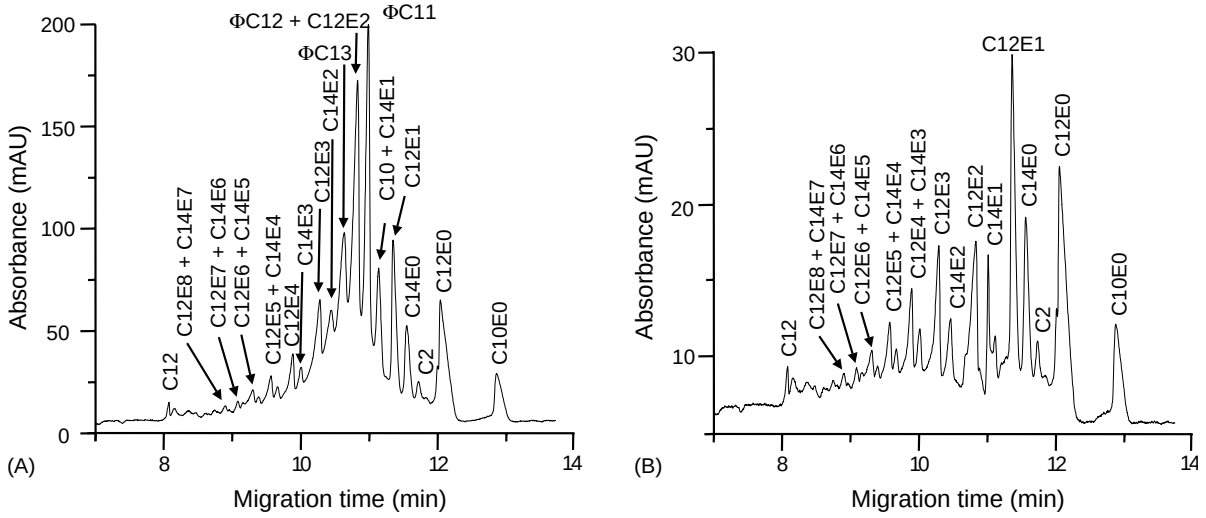


Fig. 9. Electropherograms obtained with a single injection of a soft cleaner for delicate clothes (diluted 1/35 with water); monitoring was performed with a 10 nm wide and 260 nm centred window (A), with the optimal experimental NBDW (9 nm wide and 227 nm centred) (B); 100 μg ml$^{-1}$ C10E0 added as internal standard; EOF at 6.2 min.

that corresponded to 8.5% in the undiluted sample. From the standard deviations of the residuals in the calibration curve (Fig. 6), divided by the slope, an average absolute standard deviation of $\pm 110\ \mu g\ ml^{-1}$ AES was calculated (the average relative standard deviation within the calibration range was 4.5%); this led to an estimated content of $(8.5 \pm 0.4\%)$ for this sample.

## 4. Conclusions

Both pure experimental and chemometrically supported procedures capable of removing the interference caused by any absorbing solute from electropherograms or chromatograms obtained by indirect spectrophotometric detection have been described. The NBDW procedure of Section 3.1 is extremely simple and does not require acquisition of the full two-way data matrix, nor support by chemometrics. Further, this procedure can be also implemented using a variable wavelength detector, whereas a diode array detector is required for the other two procedures described in this work. The emulated NBDW procedure of Section 3.2 involves simple chemometrics and may be of help in routine analysis, when a sample exhibits an unexpected absorbing interference. Also, it has been shown how location of the NBDW, if it exists, can be performed by means of OPA, or OPA–ALS, applied to **X**. A posteriori systematic or occasional application of the emulated NBDW procedure to routinely analysed samples (plus NBDW searching by OPA or OPA–ALS if necessary) is made possible by simply adopting the providence of storing the full spectra together with the electropherograms or chromatograms while monitoring in the optimal detection conditions.

As a probe, AQCA, has a high absorptivity maximum, and has also the advantage of showing an absorptivity minimum at the short wavelength of the ABS absorption maximum. Using AQCA, the NBDW procedures should also perform satisfactorily with many other chromophores similar to ABS, i.e. having a phenyl ring with a conjugated substituent. Other BGCs can be found to cancel the interferences produced by other absorbing solutes; however, since indirect detection sensitivity is proportional to the BGC absorptivity at the detection wavelength window, a low sensitivity will be obtained with an NBDW tailored to cancel the spectrum of a weakly absorbing solute. In these cases, OPA–ALS deconvolution provides a convenient solution with the added advantage of its universal applicability to any BGC-absorbing interference pair. Detection of NBDWs, characterisation and removal of unknown interferences, and quantitative work with both the non-absorbing and absorbing overlapped solutes can be implemented using OPA–ALS. Using a standard desktop computer, the OPA–ALS process is completed in a few minutes, and can be also programmed to be semi-automatically applied with little supervision by the user. In comparison to the NBDW procedures, OPA–ALS shows a higher susceptibility to amplify errors due to the incomplete baseline compensation. This highlights the robustness of the NBDW procedures against baseline fluctuations.

## Acknowledgements

This work was supported by Químicas Oro S.A. (Sant Antoni de Benaixever, València, Spain) and by Project BQU 2001-3047 (MCyT of Spain and FEDER funds). The support of the Generalitat Valenciana (AVCYT, CTIDIB/2002/226 and grant TS/03/05) is also acknowledged; VBZ thanks the MECD of Spain for an FPU grant, and JRTL thanks the MCyT and the University of Valencia for a Ramón y Cajal Researcher Position.

## References

[1] A. Nakae, K. Tsuji, M. Yamanaka, Anal. Chem. 53 (1981) 1818.
[2] G. Bleau, M. Desaulniers, J. Chromatogr. 487 (1989) 221.
[3] S.L. Abidi, J. Chromatogr. 362 (1986) 33.
[4] A. Marcomini, W. Giger, Anal. Chem. 59 (1987) 1709.
[5] G.R. Bear, J. Chromatogr. 459 (1988) 91.
[6] A. Marcomini, A. Di Corcia, R. Samperi, S. Capri, J. Chromatogr. 644 (1993) 59.
[7] L. Comellas, J.L. Portillo, M.T. Vaquero, J. Chromatogr. A 657 (1993) 25.
[8] Y. Yokoyama, M. Kondo, H. Sato, J. Chromatogr. 643 (1993) 169.
[9] C. Vogt, K. Heinig, B. Langer, J. Mattusch, G. Werner, Fresenius J. Anal. Chem. 352 (1995) 508.
[10] K. Heinig, C. Vogt, G. Werner, J. Chromatogr. A 745 (1996) 281.
[11] C. Crescenci, A. Di Corcia, E. Marchiori, R. Samperi, A. Marcomini, Water Res. 30 (1996) 722.
[12] K. Heinig, C. Vogt, G. Werner, Anal. Chem. 70 (1998) 1885.
[13] G. Deng, D. Chow, G. Sanyal, Anal. Biochem. 289 (2001) 124.
[14] S.H. Benomar, M.R. Clench, D.W. Allen, Anal. Chim. Acta 445 (2001) 255.
[15] G. Czichocki, H. Fiedler, K. Haage, H. Much, S. Weidner, J. Chromatogr. A 943 (2002) 241.
[16] J. Bullock, J. Chromatogr. 645 (1993) 169.
[17] S.A. Shamsi, N.D. Danielson, Anal. Chem. 66 (1994) 3757.
[18] H. Salimi-Moosavi, R.M. Cassidy, Anal. Chem. 68 (1996) 293.
[19] G.M. McLaughlin, A. Weston, K.D. Hauffe, J. Chromatogr. A 744 (1996) 123.
[20] K. Heinig, C. Vogt, G. Werner, J. Cap. Electroph. 3 (1996) 261.
[21] A. Monclus, M. Rodriguez, I. Masana, LC–GC Int. 9 (1996) 79.
[22] K. Heinig, C. Vogt, Fresenius J. Anal. Chem. 359 (1997) 202.
[23] K. Heinig, C. Vogt, G. Werner, Fresenius J. Anal. Chem. 357 (1997) 695.
[24] C. Vogt, K. Heinig, Tenside Surf. Det. 35 (1998) 470.
[25] K. Heinig, C. Vogt, G. Werner, Analyst 123 (1998) 349.
[26] W.H. Ding, C.H. Liu, J. Chromatogr. A 929 (2001) 143.
[27] J.M. Herrero-Martínez, E.F. Simó-Alfonso, G. Ramis-Ramos, Electrophoresis 22 (2001) 2017.
[28] J.M. Herrero-Martínez, E.F. Simó-Alfonso, C. Mongay-Fernández, G. Ramis-Ramos, J. Chromatogr. A 895 (2000) 227.
[29] J.M. Herrero-Martínez, M. Fernández-Martí, E.F. Simó-Alfonso, G. Ramis-Ramos, Electrophoresis 22 (2001) 526.
[30] M. Grob, F. Steiner, Electrophoresis 23 (2002) 1921.
[31] J.M. Herrero-Martínez, E.F. Simó-Alfonso, G. Ramis-Ramos, Electrophoresis 24 (2003) 681.
[32] J. Zweigenbaum, J. Chromatogr. 11 (1990) 9.

[33] P.L. Desbene, C.M. Rony, B. Desmazieres, J.C. Jacquier, J. Chromatogr. 608 (1992) 375.
[34] S. Chen, D.J. Pietrzyk, Anal. Chem. 65 (1993) 2770.
[35] R. Loos, J. Riu, M.C. Alonso, D. Barcelo, J. Mass Spectrom. 35 (2000) 1197.
[36] M.W.F. Nielen, J. Chromatogr. 588 (1991) 321.
[37] K. Heinig, C. Vogt, Fresenius J. Anal. Chem. 363 (1999) 612.
[38] K. Heinig, C. Vogt, Electrophoresis 20 (1999) 3311.
[39] V. Zuriguel, E. Causse, J.D. Bounery, G. Nouadje, N. Simeon, M. Nertz, R. Salvayre, F. Couderc, J. Chromatogr. A 781 (1997) 233.
[40] O. Schmitz, D. Melchior, W. Schuhmann, S. Gäb, J. Chromatogr. A 814 (1998) 261.
[41] D. Melchior, S. Gäb, J. Chromatogr. A 894 (2000) 145.
[42] I. Miksik, Z. Deyl, J. Chromatogr. A 807 (1998) 111.
[43] E. Drange, E. Lundanes, J. Chromatogr. A 771 (1997) 301.
[44] T. Wang, H. Wei, S.F.Y. Li, Electrophoresis 19 (1998) 2187.
[45] M.J. Chen, H.S. Chen, C.Y. Lin, H.T. Chang, J. Chromatogr. A 853 (1999) 171.
[46] D.L. Gallaher Jr., M.E. Johnson, Anal. Chem. 72 (2000) 2080.
[47] A. Dermaux, P. Sandra, V. Ferraz, Electrophoresis 20 (1999) 74.
[48] J. Collet, P. Gareil, J. Chromatogr. A 792 (1997) 165.
[49] R. Roldan-Assad, P. Gareil, J. Chromatogr. A 708 (1995) 339.
[50] F.B. Erim, X. Xu, J.C. Kraak, J. Chromatogr. A 694 (1995) 471.
[51] A. Desbène, C.J. Morin, N.L. Mofaddel, R.S. Groult, J. Chromatogr. A 716 (1995) 279.
[52] P. L Desbène, C.J. Morin, Spectra Anal. 25 (1996) 15.
[53] V. Bernabé-Zafón, S. Ortega-Gadea, E.F. Simó-Alfonso, G. Ramis-Ramos, Electrophoresis 24 (2003) 2805.
[54] F. Cuesta-Sánchez, B. van den Bogaert, S.C. Rutan, D.L. Massart, Chemom. Intell. Lab. Syst. 34 (1996) 139.
[55] F. Cuesta-Sánchez, J. Toft, B. van den Bogaert, D.L. Massart, Anal. Chem. 68 (1996) 79.
[56] R. Tauler, D. Barceló, Trends Anal. Chem. 12 (1993) 319.
[57] H. Li, F. Zhang, J. Havel, Electrophoresis 24 (2003) 3107.
[58] C.Y. Airiau, R.G. Brereton, S. Dunkerley, Analyst 125 (2000) 833.
[59] R. Bro, N.D. Sidiropoulos, J. Chemom. 12 (1998) 223.